ADVANCED FUNCTIONAL MATERIALS

Supporting Information

for *Adv. Funct. Mater.,* DOI: 10.1002/adfm.202103511

Engineering DNA-Grafted Quatsomes as Stable Nucleic Acid-Responsive Fluorescent Nanovesicles

Marianna Rossetti, Lorenzo Stella, Judit Morlà-Folch, Sara Bobone, Ariadna Boloix, Lorena Baranda, Danila Moscone, Mònica Roldán, Jaume Veciana, Miguel F. Segura, Mariana Köber, Nora Ventosa,* and Alessandro Porchetta**

Supporting Information

Engineering DNA-grafted Quatsomes as Stable Nucleic acid-Responsive Fluorescent Nanovesicles

Marianna Rossetti, Lorenzo Stella, Judit Morla-Folch, Sara Bobone, Ariadna Boloix, Lorena Baranda, Danila Moscone, Mònica Roldán, Jaume Veciana, Miguel F. Segura, Mariana Köber, Nora Ventosa*, Alessandro Porchetta**

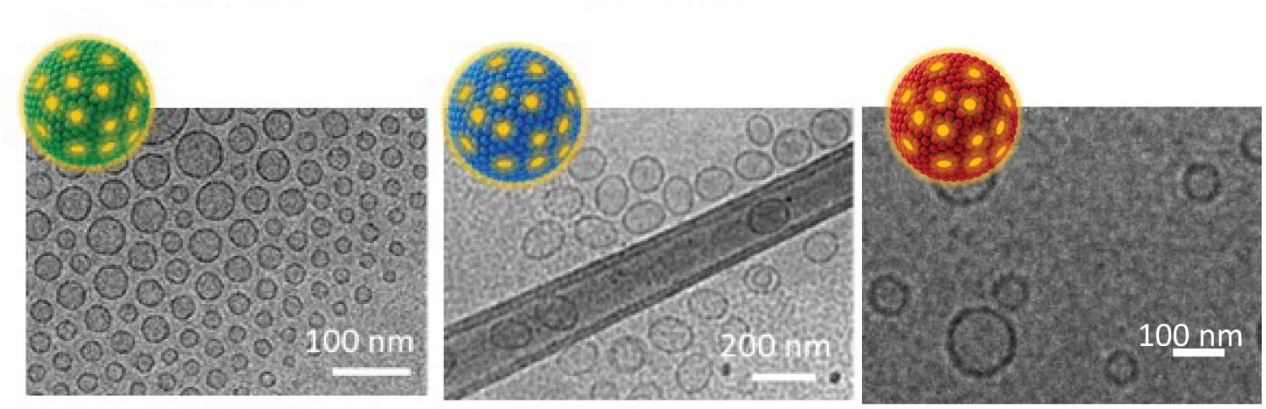

Figure S1. Cryo-transmission electron microscopy (CryoTEM) images of Quatsome vesicles (synthon concentration here is 1.3 mM) produced by DELOS-SUSP and measured the one month after of production. From right to left, QS(++)/DiI (green particle), QS(+)/DiI (blue particle) and QS(-)/DiI (red particle). Scale bars are reported in the images.

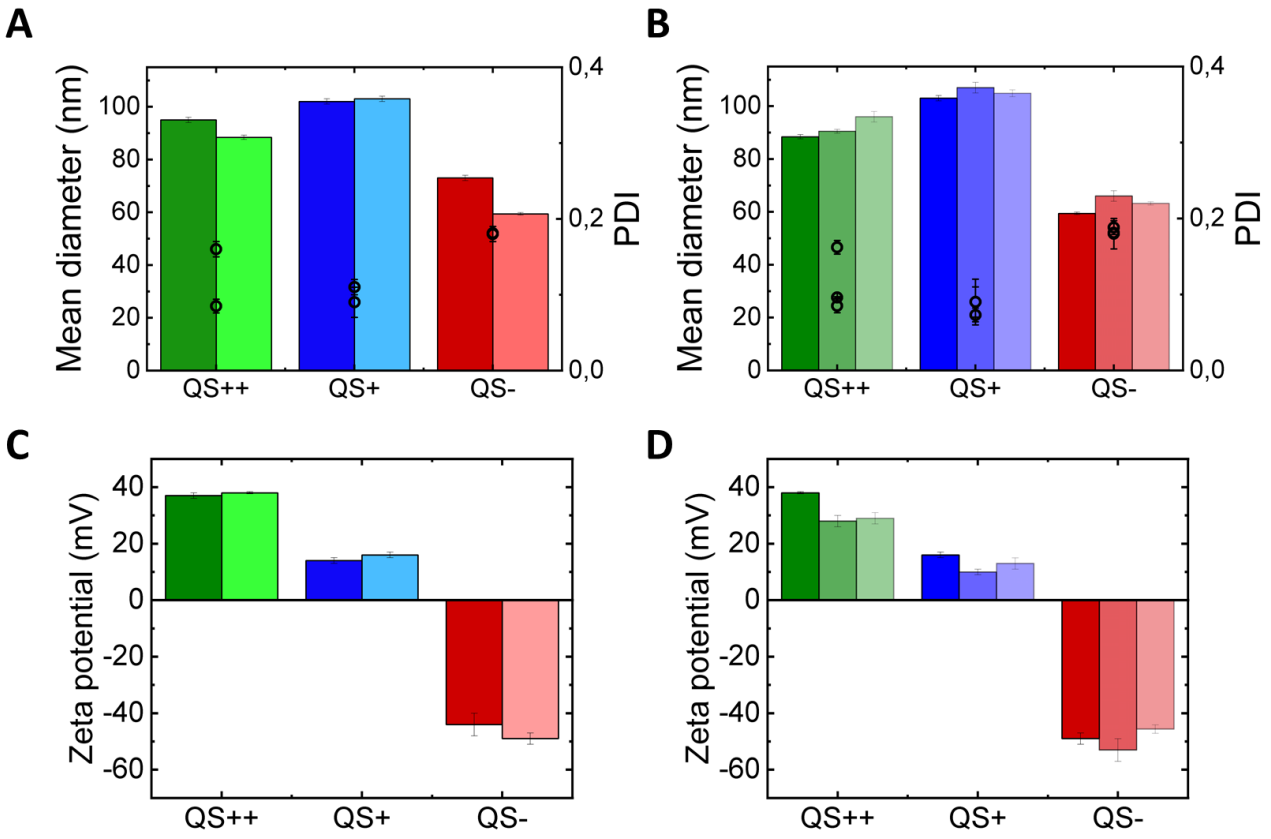

Figure S2. Batch-to-batch reproducibility and temporal stability of vesicle size and zeta potential. A-B) Intensity weighted mean hydrodynamic diameter and polydispersity index (PDI), measured by Dynamic Light Scattering. **C-D**) Zeta potential, measured by Electrophoretic Light Scattering. **A)** and **C)** Mean diameter, PDI and zeta potential of two different batches, obtained one week after production. **B)** and **D)** Mean diameter, PDI and zeta potential obtained measuring the same batch at different time points after production, namely after 1 week (dark colors, left columns), 4 months (medium tones, middle columns), and 10 months (light colors, right columns). Error bars represent the standard deviation of three measurements of the same sample.

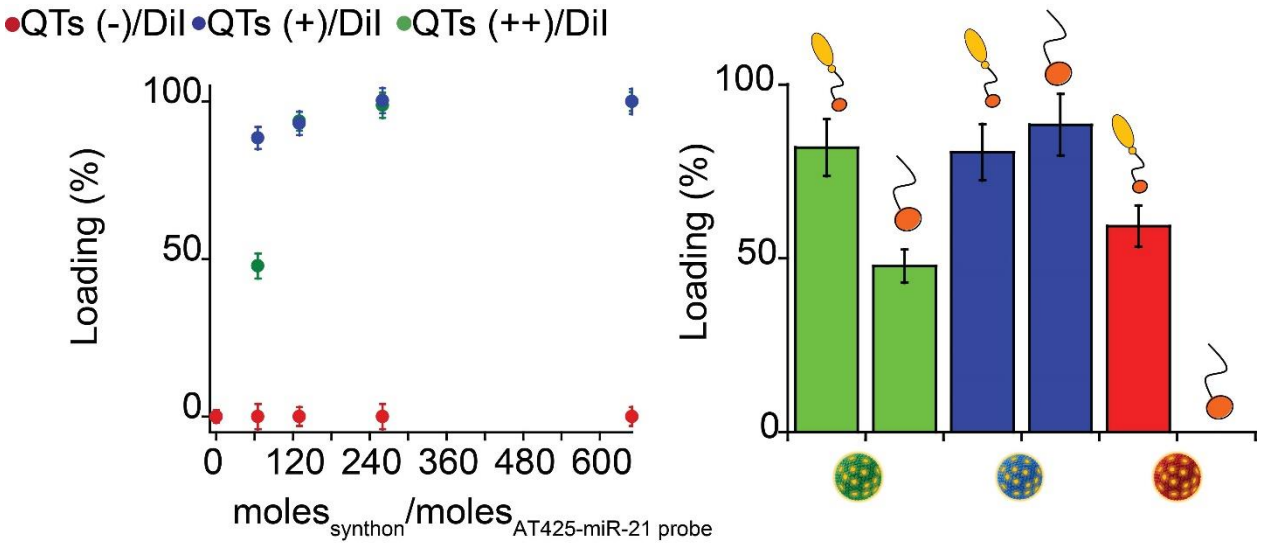

Figure S3. Left) Loading of AT425-miR-21 probe on QS vesicles performed through fluorescence assays using a fixed concentration of AT425-miR-21 probe without cholesterol (AT425-miR-21 probe w/o chol. 100nM) and increasing concentrations of synthon. We calculated Loading (%) from the fluorescence intensity (see experimental section for further details). **Right**) Comparison of the Loading (%) values obtained using AT425-miR-21 probe and AT425-miR-21 probe w/o chol. at the ratio moles $_{\text{synthon}}$/moles $_{\text{AT425-miR-21 probe}}$ equal to 65, highlighting the effect of the cholesterol moiety on the vesicle functionalization.

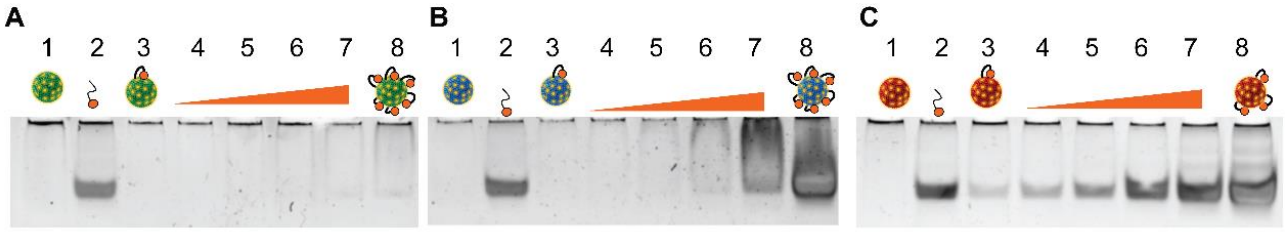

	Line							
	1	**2**	**3**	**4**	**5**	**6**	**7**	**8**
Synthon [µM]	26	-	26	26	26	26	26	26
AT425-miR-21 probe [µM]	-	0.3	0.025	0.05	0.1	0.3	1	3

Figure S4. Polyacrylamide gel assays of quatsome nanovesicles (synthon 130 µM) pre-incubated with different concentrations of AT425-miR-21 probe w/o cholesteryl-TEG moiety. **A)** QS(++)/DiI/AT425-miR-21 probe w/o cholesterol; **B)** QS(+)/DiI AT425-miR-21 probe w/o cholesterol; **C)** QS(-)/DiI AT425-miR-21 probe w/o cholesterol.

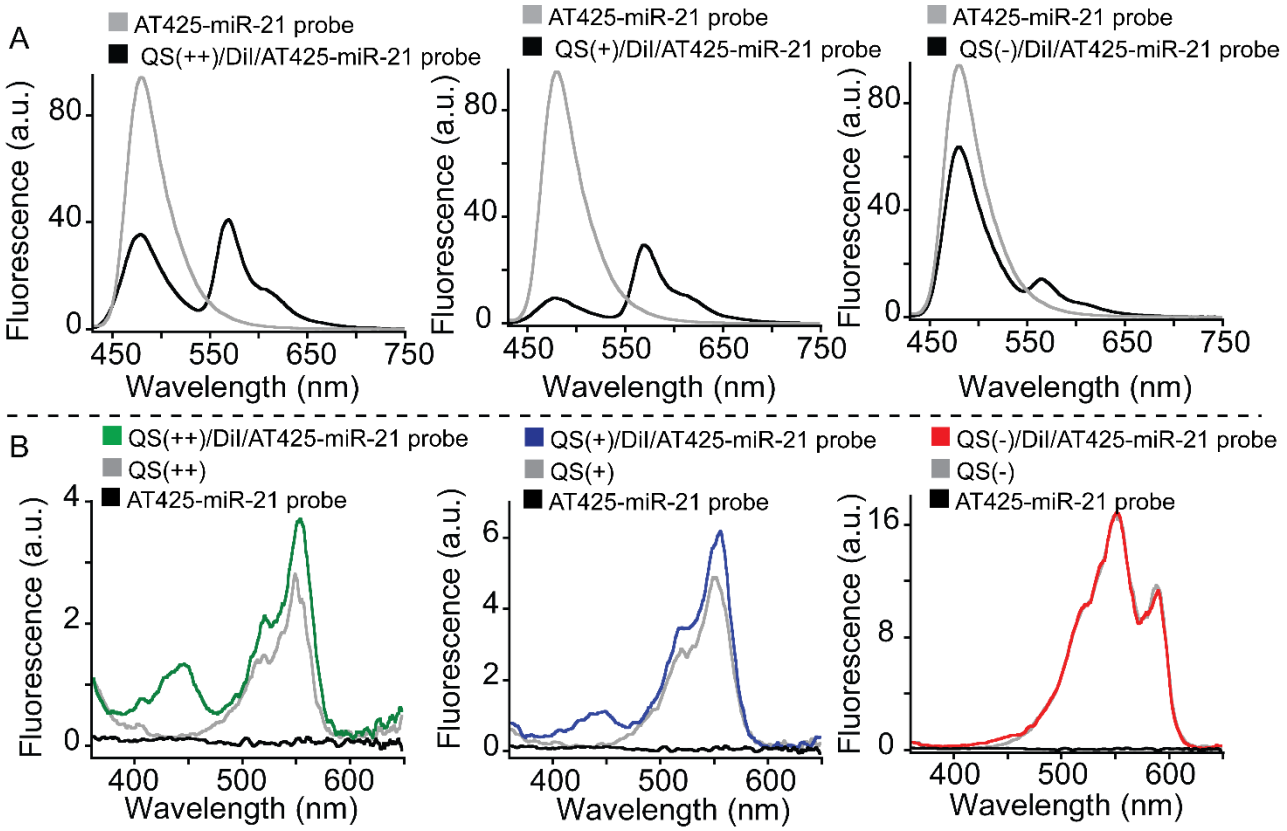

Figure S5. Photophysical properties of the QS/DiI vesicles modified with AT425/ miR-21 probe. Here, AT425 conjugated to the miR-21 probe acts as FRET donor and embedded DiI fluorophore in QS vesicle acts as acceptor. Fluorescence emission and excitation spectra demonstrate significant FRET only for positive QSs (QS(++)/DiI/AT425-miR-21 probe and QS(+)/DiI/AT425-miR-21 probe). Although a decrease in the fluorescent emission of the ATTO425 donor and an increase in the DiI emission is present also in QS(-)/DiI/AT425-miR-21 probe, excitation spectra obtained at λ_{em} = 620 nm indicate that no significant energy transfer is present. **A)** Emission spectra of QS(++), left; QS(+), middle; QS(-), right; obtained by exciting AT425 of AT425-miR-21 probe (200 nM) as donor in the presence and in the absence of a fixed concentration of synthon (i.e. 26 μM) (λ_{exc} = 430 nm). **B)** Excitation spectra obtained at λ_{em} = 620 nm showing efficient energy transfer only for QS(++)/DiI/AT425-miR-21 probe and QS(+)/DiI/AT425-miR-21 probe.

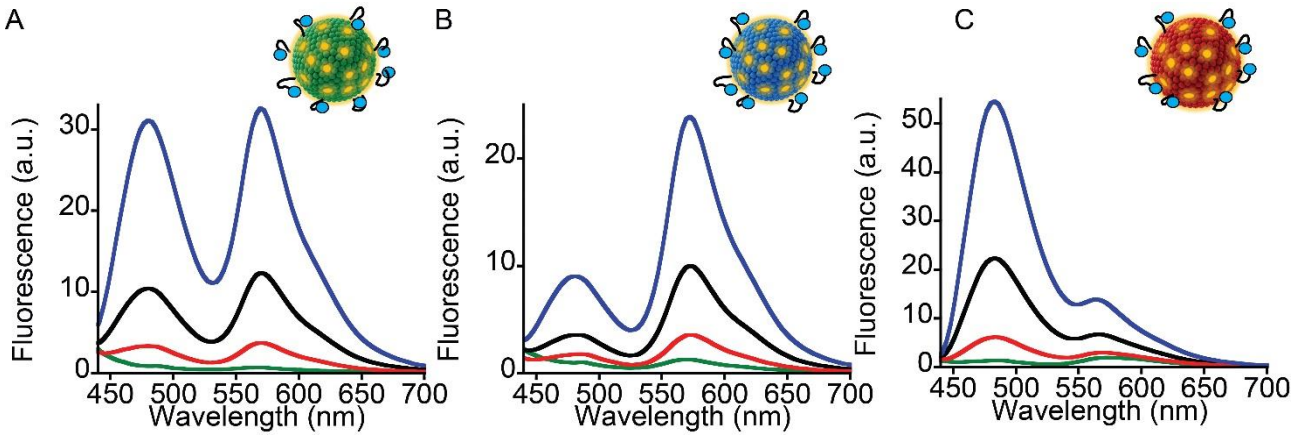

Figure S6. Effect of donor concentration on the FRET signals of the system. We tested increasing concentration of AT425/miR-21 probe anchored on DiI-loaded QS vesicles to evaluate the effect on the FRET signal due to the increase in the donor concentration (AT425). Emission spectra obtained **A)** QS(++)/DiI/ AT425/miR-21 probe, **B)** QS(+)/DiI/AT425/miR-21 probe, **C)** QS(-)/DiI/ AT425/miR-21 probe by exciting AT425 (λ_{exc} = 430 nm). Green lines show the spectra of only QS/DiI (without AT425-miR-21 probe); in red, QS functionalized with AT425-miR-21 probe at concentration 25 nM; in black, QS functionalized with AT425-miR-21 probe at concentration 100 nM; in blue, QS functionalized with AT425-miR-21 probe at concentration 200 nM.

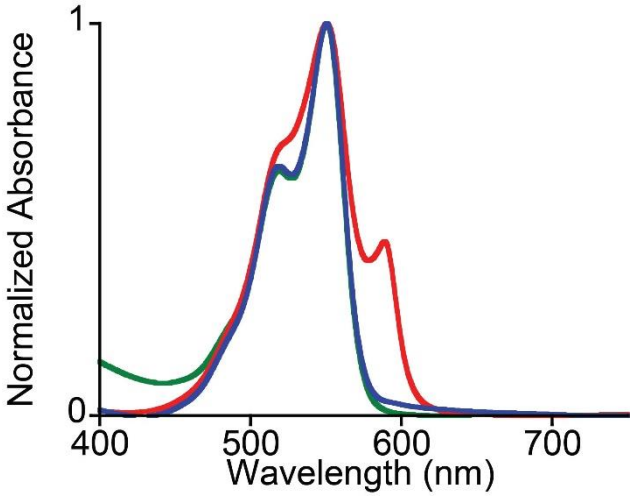

Figure S7. Absorption spectra of QS(++)/DiI (green line), QS(+)/DiI (blue line) and QS(-)/DiI (red line). To allow for more ready interpretation of the results, we normalized absorbance signals (right) on a 0−1 scale using the following formula: Normalized Absorbance = = $\frac{A-A_0}{A_{max}-A_0}$, where A_{max} represents the maximum absorbance signal (Rel. Abs. =1), whereas A_0 is the minimum signal (Rel. Abs. = 0).

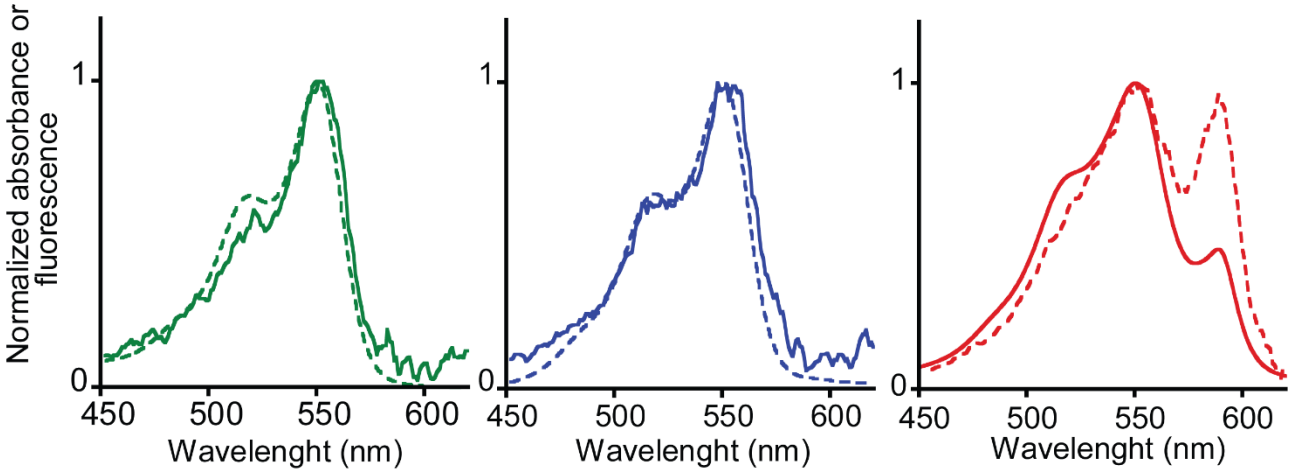

Figure S8. Normalized excitation (solid line) and absorption (dashed line) spectra of QS(++)/DiI (left), QS(+)/DiI (middle) and QS(-)/DiI (left). To allow for more ready interpretation of the results, we normalized absorbance and fluorescence signals on a 0−1 scale. We recorded excitation spectra by fixing the emission at 700 nm and collected data from 450 nm and 620 nm

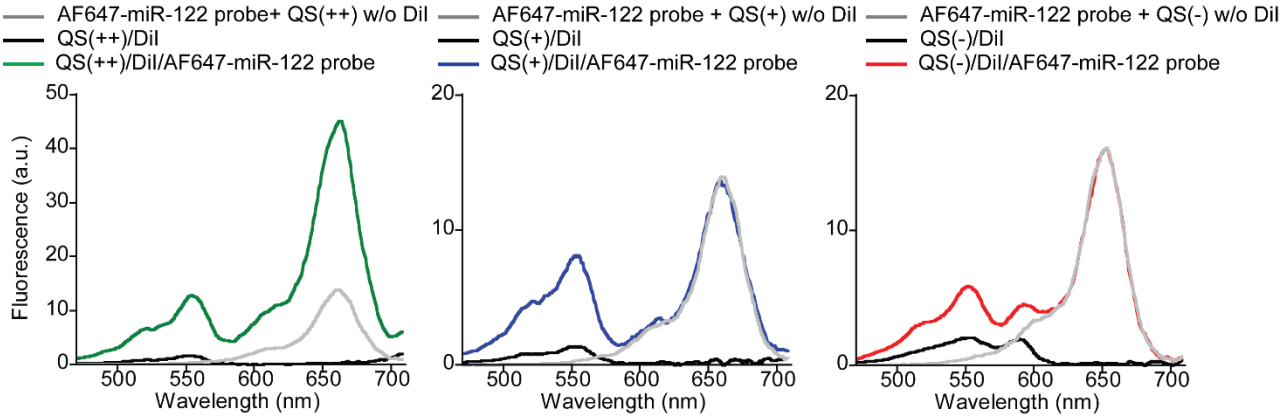

Figure S9. Excitation spectra, demonstrating that FRET mechanism occurs in the three QS/DiI/AF647-miR-122 probe systems. Here, we reported the excitation spectra of QS/DiI (at concentration of synthon equal to 26 µM) before (black lines) and after the functionalization with AF647-miR-122 probe (at concentration equal to 200 nM, curves in green, blue and red). In gray the spectra obtained by incubating QS vesicles (without DiI) and AF647-miR-122 probe in the same previous concentrations. Fluorescence signals collected at λ_{em} = 750 nm for the three systems (QS(++)/DiI/AF647-miR-122 probe, left; QS(+)/DiI/AF647-miR-122 probe, middle and QS(-)/DiI/ AF647-miR-122 probe, right) show an increase in the emission associated to DiI absorption (~ 555 nm), thus confirming FRET from DiI (donor) loaded on QSs when in the presence of AF647-labelled miR-122 probe.

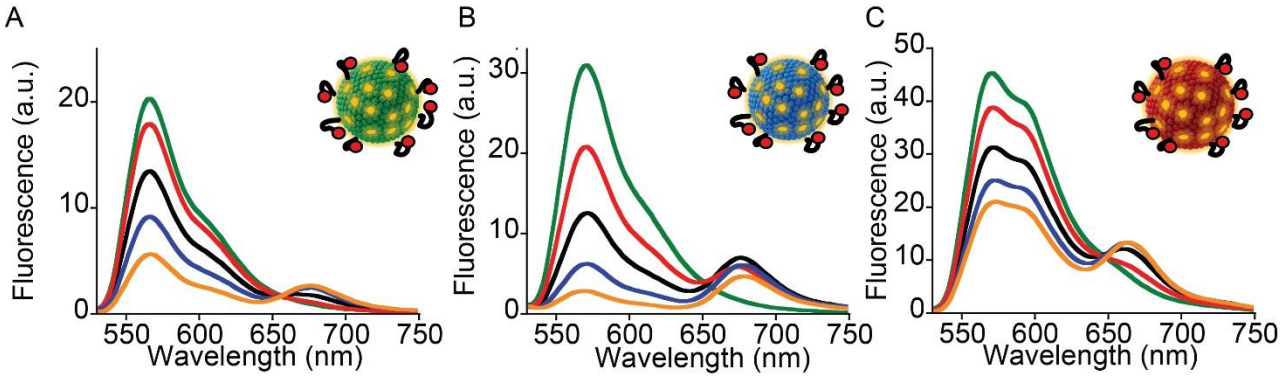

Figure S10. Emission spectra of **A)** QS(++)/DiI/AF647-miR-122 probe; **B)** QS(+)/DiI/AF647-miR-122 probe; **C)** QS(-)/DiI/AF647-miR-122 probe using a fixed concentration of Quatsome (synthon at concentration equal to 26 µM) and by adding increasing concentrations of AF647-miR-122 probe (λ_{exc} = 520 nm): green (without AF647-miR-122 probe), red (30 nM), black (100 nM), blue (200 nM), orange (300 nM). By increasing the concentration of the DNA probe a decrease of the donor emission (DiI) and an increase of the acceptor fluorescence (AF647) is observed.

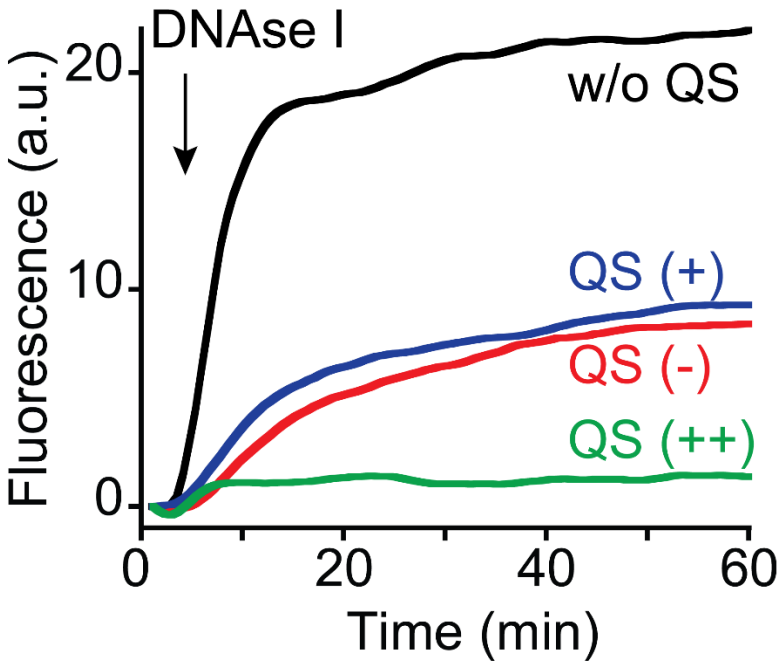

Figure S11. Nuclease activity assays using non-labelled QS vesicles functionalized with chol-TEG-miR-122 probe internally labelled with a FRET pair (AT425/AT550). Here, 10 µg of DNAse I were added in 45 µL of solution containing 30 nM of miR-21 probe dual labelled (black lines) and to solutions containing the same probe pre-incubated with QS nanovesicles not containing DiI at synthon concentration equal to 26 µM (in blue QS(+), in red QS(-), in green QS(++)) .

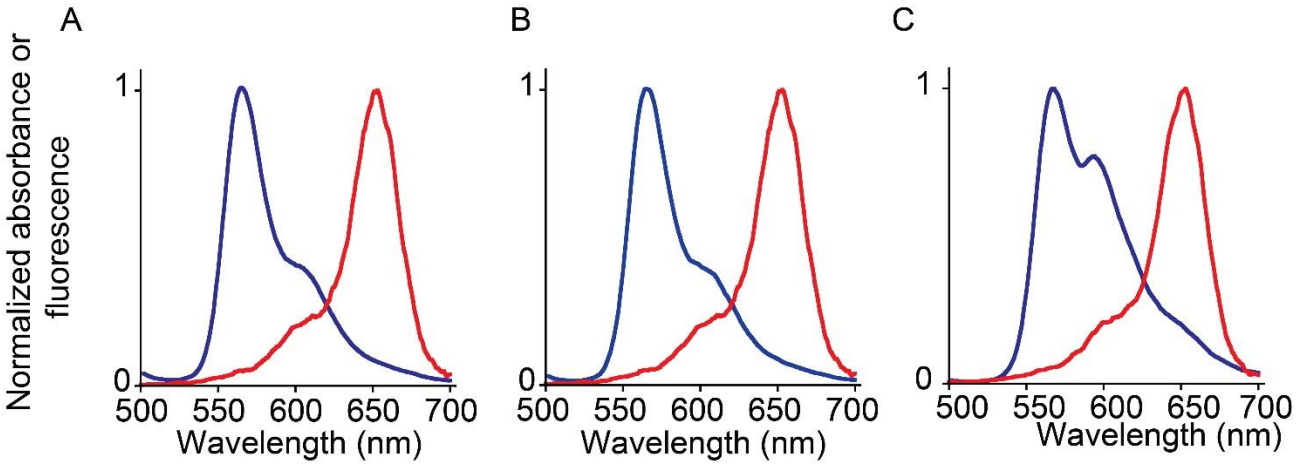

Figure S12. Normalized spectra used for for the calculation of Förster radius (see experimental section). Blue lines represent the emission spectra of DiI embedded in A) QS(++), B) QS(+) and C) QS(-) acting as donor. In red, the corresponding absorption spectra of AF647 working as acceptor.

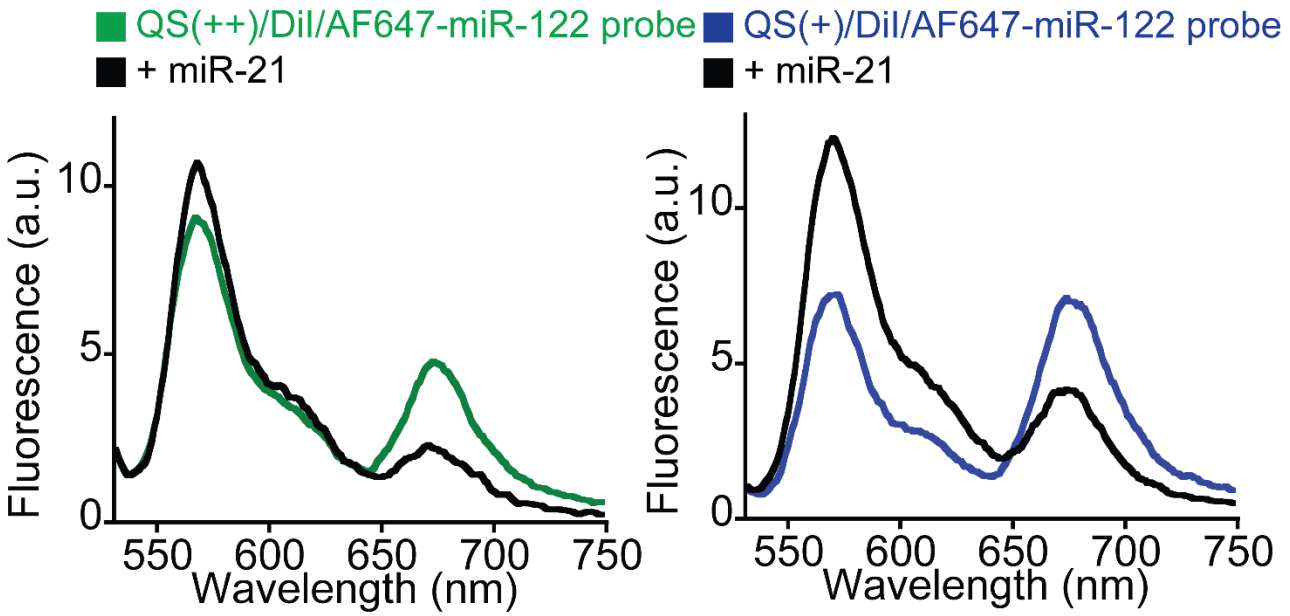

Figure S13. Fluorescence spectra of QS(++)/DiI/AF647-miR-122 w/o cholesterol probe (left) and QS(+)/DiI/AF647-miR-122 w/o cholesterol probe in the presence (colored lines) by adding a non-specific target RNA (i.e. [miR-21] = 100 nM). The spectra indicate a change in FRET efficiency in the presence of the non-specific miRNA target. These data thus indicate that cholesterol is necessary to achieve specific miR-122 detection as this behavior was not observed for QSs where the miRNA probe included a cholesteryl moiety (Figure 3).

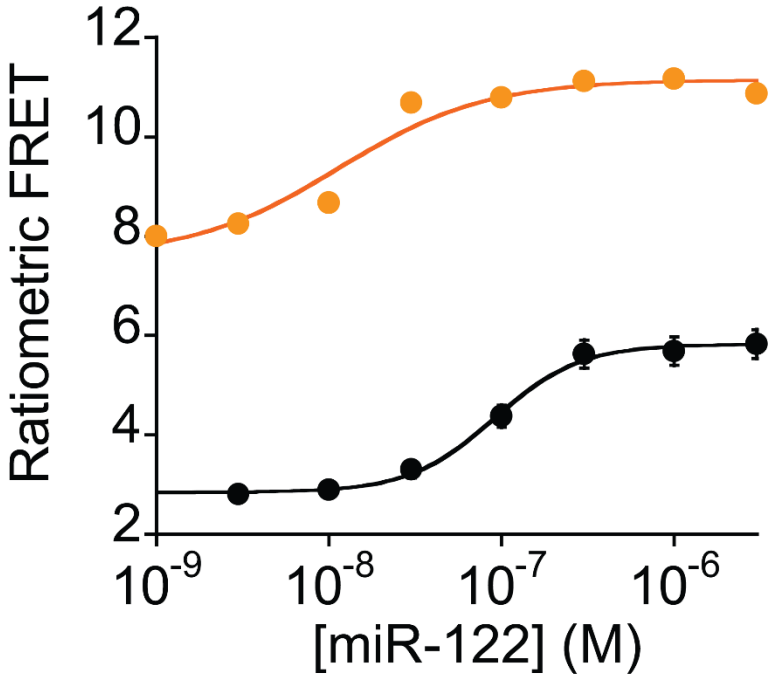

Figure S14. Binding curves obtained by adding increasing concentration of miR-122 to a solution containing a fixed concentration of QS(-)/DiI (26 µM of synthon) pre-incubated with 200 nM of AF647-miR-122 probe (black curve) or 30 nM of AF647-miR-122 probe (orange curve). A shift in the apparent binding affinity is observed ($K_{1/2,\ black}$ = 90 ± 10 nM; $K_{1/2,\ orange}$ = 11 ± 7 nM). This finding can be explained in terms of probe concentration anchored on the surface of the particles.

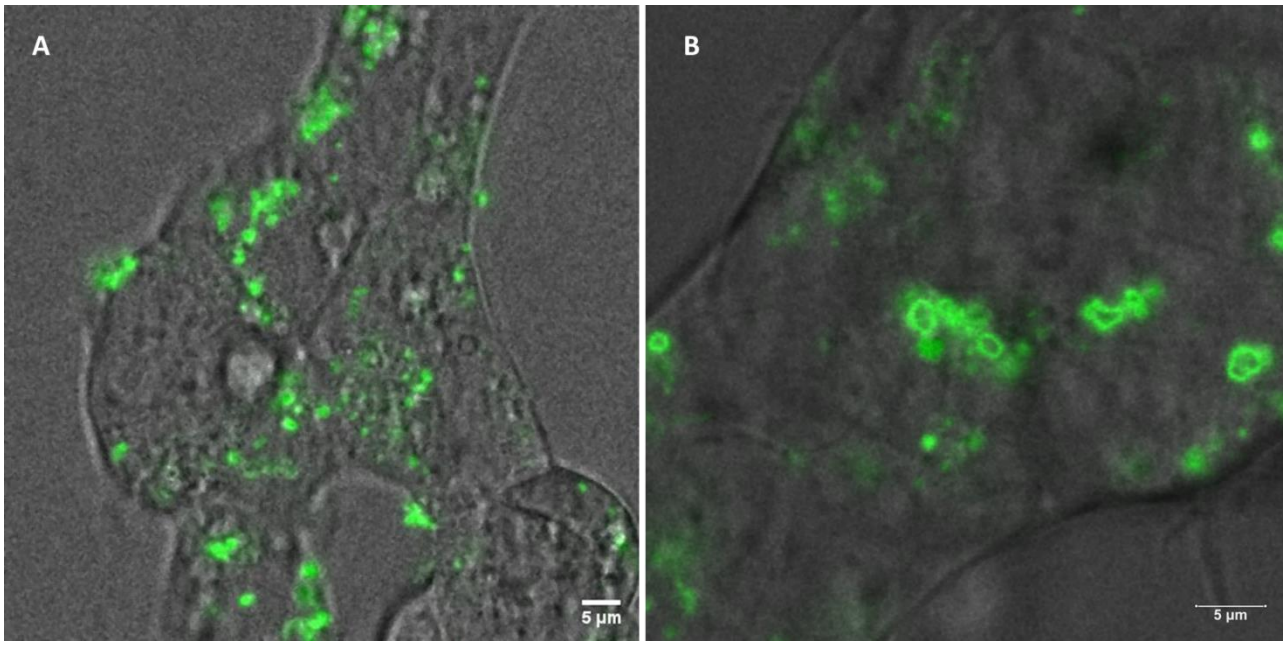

Figure S15. Cell penetrability of DNA-grafted QS(+)/DiI and QS(++)/DiI. Representative confocal images of HEK293T cells incubated with DNA-grafted QS/DiI (green channel) and merged with transmitted light (gray channel), showing the detection of QS accumulated inside the cell. **A)** QS(+/DiI/AF647-miR-122 probe. **B)** QS(++)/DiI//AF647-miR-122 probe. Scale bars= 5µm.

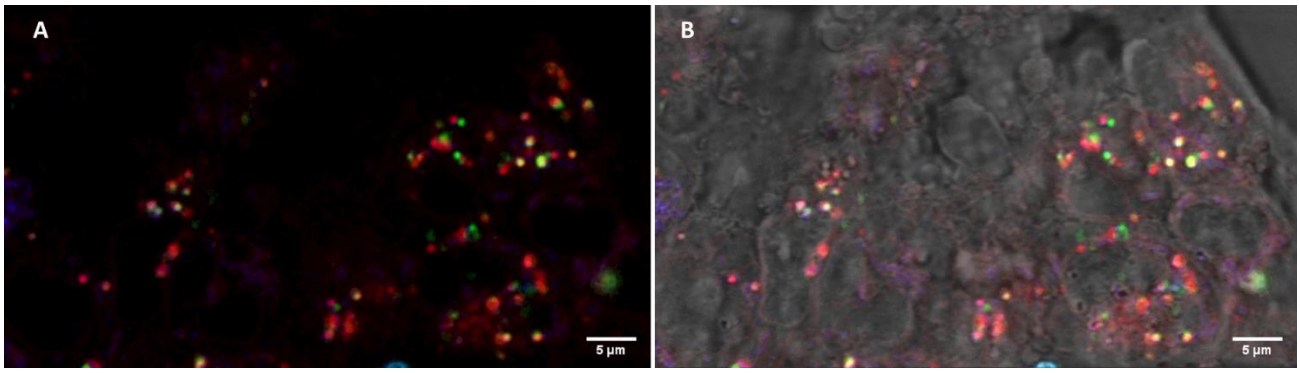

Figure S16. Cell internalization of DNA-grafted QS(+) and lysosome colocalization. A) Representative confocal image of HEK293T cells incubated with QS(+) grafted with miR-21 probe, dual-labelled with ATTO425 and ATTO550 (blue and green channels, respectively). Only partial colocalization with lysosomes, stained with Lysotracker Deep Red (red channel), suggests the delivery of DNA-grafted QS(+) to the cytosol. **B)** Image shown in A), merged with transmitted light (gray channel), showing the detection of QS accumulated inside the cell. Scale bars = 5 µm.

QS	Synthon concentration [mM]	Dye Concentration [µM][a)]	Hydrodynamic diameter [nm][b)]	PdI[b)]	ζ-potential [mV][b)]	QS concentration (10^{12} particles/mL)[c)]	Estimated Number of DiI molecules per QS	Surface area per DiI molecule [nm^2]
QS(++)	1.3	8.2	92±3	0.12±0.04	37±1	9.2	534	93
QS(+)	1.3	15.5	102±1	0.10±0.01	15±1	7.6	1200	49
QS(-)	1.3	44.5	66±7	0.18±0.01	-47±3	20	1300	18

[a)] DiI concentration incorporated into the vesicles was determined by absorption measurements (Lambert-Beer law). [b)] Mean values and standard deviation of hydrodynamic size (diameter), polydispersity index and ζ-potential of two different QS batches, each measured one week after production by Dynamic Light Scattering (DLS) and Electrophoretic Light Scattering, respectively. [c)] QS concentration was estimated as follows: the surface of the outer and inner leaflets of the bilayer was calculated from the particle diameter and considering a previously determined bilayer thickness of 4.4 nm,[1] assuming a spherical shape. The surface area for a synthon was estimated from molecular dynamics simulations to be 0.58 nm^2 for all QSs.[1] Dividing the total QS surface area by the area per synthons, the number of synthons per QS was obtained 85000, 100000, 40000 for QS(++), QS(+) and QS(-), respectively). The QS concentration was finally obtained by dividing the cholesterol or surfactant molar concentration by the number of molecules per QS.

Table S1. Physicochemical properties of QSs loaded with DiI

QS	λ_{max} abs [nm][a)]		λ_{max} emi [nm]		Φ_F[b)]	FRET efficiency [%][c)]	
	DiI	AF647	DiI	AF647	DiI	w/o miR-122	with miR-122
QS(++)	552	660	565 605	675	0.32	80	69
QS(+)	552	660	565 605	675	0.22	60	42
QS(-)	552 590	660	565 595 645	665	0.20	25	14

[a)]Absorption and emission maxima ±1 nm. [b)]Fluorescence quantum yield of DiI measured in the QSs but in the absence of AF647-miR-122 probe ±10%. [c)]FRET efficiency calculated from the decrease in donor's (DiI) steady state fluorescence in presence and absence of target miR-122 (1 μM).

Table S2. Photophysical properties of QS/DiI vesicles

QS	Φ_F [%][a)]	ε [M^{-1} cm^{-1}][b)]	Brightness [10^3 M^{-1} cm^{-1}][c)]	Estimated num. molecules/QS[d)]	ε_p [10^6 M^{-1} cm^{-1}][e)]	$Brightness_p$ [10^6 M^{-1} cm^{-1}][f)]
QS(++)	32	140000	45	540	76	24
QS(+)	22	140000	31	1700	240	53
QS(-)	20	140000	28	1500	210	42

[a)]DiI fluorescence quantum yield ± 10%. [b)]Molar extinction coefficient of DiI at the maximum absorption wavelength. [c)]Brightness of DiI calculated as $\varepsilon \times \phi_F$. [d)]Estimated number of DiI molecules per quatsome calculated from the concentration of dye and the concentration of QSs (see Table S1). [e)]Molar extinction coefficient at the maximum absorption wavelength of a single QS, calculated as $\varepsilon \times n$, where n is the estimated number of fluorophores per vesicle. [f)]Brightness of a single fluorescent quatsome calculated as $\varepsilon_p \times \phi_F$

Table S3. QS brightness.

QS	LoD[a)] (nM)	Linear Dynamic Range (nM)	Sensitivity (ratiometric FRET/nM)	Response time
QS(++)	60	200-1000	0.0035	5 min
QS(+)	40	100-300	0.0042	5 min
QS(-)	30	80-100	0.0162	5 min

[a)]Limit of Detection calculated as 3.3*Std of ratiometric FRET in the absence of target/ Slope of ratiometric FRET *vs*. Target concentration

Table S4. Analytical Parameters of active DiI-loaded QS nanovesicles for miRNA detection.

Reference

[1] L. Ferrer-Tasies, E. Moreno-Calvo, M. Cano-Sarabia, M. Aguilella-Arzo, A. Angelova, S. Lesieur, S. Ricart, J. Faraudo, N. Ventosa, J. Veciana, *Langmuir* **2013**, *29*, 6519.